Proc. of IEEE ISPLC 2014, Glasgow, March 2014

Performance of MIMO PLC in Measured Channels Affected by Correlated Noise

Alberto Pittolo, Andrea M. Tonello, and Fabio Versolatto
WiPli Lab – Wireless and Power Line Communications Lab
University of Udine – Via delle Scienze 208, 33100 Udine, Italy
Email: {alberto.pittolo, tonello, fabio.versolatto}@uniud.it

***Abstract*—We study the performance improvement provided by the use of precoding schemes in multiple-input multiple-output (MIMO) power line communications (PLC) in the presence of additive colored and correlated Gaussian noise. We assume a power spectral density constraint, according to the HomePlug AV2 standard, and we focus on a 2×4 MIMO system, thus exploiting also the common mode at the receiver side. The MIMO channels have been obtained through an experimental measurement campaign across Europe, collected by the ETSI special task force 410. We compare the performance (in terms of capacity) when the power allocation is optimal or uniform. Furthermore, a comparison with the single-input single-output (SISO) and reduced-dimension MIMO configurations is made, showing as the 2×4 MIMO scheme outperforms the others.**

Keywords*—Power line communications (PLC), multiple-input multiple-output (MIMO), correlated noise, colored noise, experimental measures

I. Introduction

Power line communications (PLC) is an established solution to convey high speed data content exploiting the existent power delivery infrastructure. Recent PLC standards, as Home Plug AV2 [1], ensure data rates of about 500 Mbps at the PHY layer. Such a high throughput is obtained by signaling in the extended frequency band between 2–86 MHz, making use of advanced multicarrier modulation schemes based on orthogonal frequency division multiplexing (OFDM), and by enabling the use of multiple-input multiple-output (MIMO) solutions to further extend coverage or to provide higher data rates w.r.t. more conventional single-input single-output (SISO) PLC. Basically, a 2×4 MIMO communication can be established by exploiting the presence of multiple conductors, namely three. They are the phase (P), the neutral (N) and the protective earth (E). The latter provides a return path for the power supply short-circuit alternated currents (50 Hz) that take place in the presence of an insulation fault.

At the transmitter side, the signal is injected between pairs of wires. The transmission modes are referred to as delta, Δ. Due to the Kirchhoff's laws, only two Δ signals can be injected at the same time. At the receiver, the signal is observed between one conductor and a reference plane. The configuration is referred to as star-style and the number of star-style modes is three, as the number of wires. See the scheme depicted in Fig. 1. Furthermore, coupling between the wires and the physical earth, due to unbalanced parasitic capacities from grounded devices, can be exploited to get another receiver mode, namely the common mode (CM) [2]. Basically, the CM flows with the same intensity and direction through P, N and E. With CM, the number of available modes at the receiver port is four (see Fig. 1). Due to EMI reasons, the common mode is used only at the receiver side.

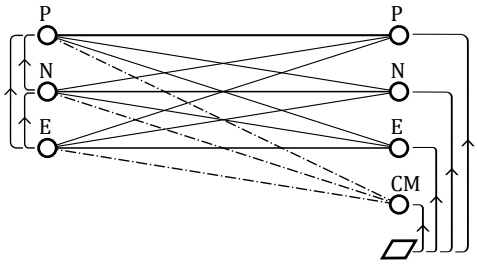

Fig. 1. MIMO modes according to STF-410.

A preliminary analysis of the performance improvement achieved through the use of a 2×4 MIMO communication method, compared to the SISO system, in the 4–30 MHz frequency band is reported in [3]. Herein, additive white Gaussian noise (AWGN) is assumed and spatial multiplexing, through beamforming at the transmitter side and zero forcing (ZF) detection at the receiver, is discussed. Under the same system assumptions, precoded spatial multiplexing is considered in more detail in [4], while [5] describes implementation and results of the MIMO PLC feasibility study. Otherwise, this paper investigates the effects on the MIMO PLC channel capacity due to the detrimental effect of colored and correlated noise (rather than AWGN), as well as the performance improvement provided by the frequency extension up to 86 MHz. The 2×4 Δ-star MIMO communication channel is considered. An extension to the 0–100 MHz frequency band, end the assumption of colored noise, instead of white noise, is already done in [6]. However, in this case, the 2×2 MIMO channel with a Δ-style mode configuration, at both the transmitter and the receiver ends, is taken into account.

The purpose of this paper is to evaluate the MIMO PLC performance in the extended frequency range 2–86 MHz, foreseen by the latest PLC standards [1] for the next generation PLC systems. A comparison is performed between different MIMO configurations and precoding schemes, taking into account a 2×4 MIMO communication channel, thus, exploiting the additional CM at the receiver. The focus is on a Δ-style feeding mode and a star-style receiving mode. Furthermore, the presence of a colored (in frequency) and correlated (between different receiving modes) Gaussian noise is assumed. Concerning the channel, we exploit the database that was collected by the special task force 410 (STF-410)

of the European telecommunication standardization institute (ETSI) during an experimental measurement campaign across Europe [2]. This allows us to obtain fair results which estimate with good approximation the performance of real PLC networks. The measurements were performed in the 1–100 MHz frequency range. We provide a concise statistical analysis of the channels [7]. Namely, we study the cumulative distribution function of the average channel gain (ACG) and the mean value of the eigen-spread as a function of frequency. Concerning the noise, we model it from the experimental results reported in [7] and [8]. It should be noted that in [7] the channel capacity distribution is evaluated assuming an equal PSD constraint over the whole frequency range, as well as an uncorrelated AWGN noise. Otherwise, we consider a PSD constraint according to the HomePlug AV2 standard [1], as specified in Section IV, and a colored and correlated noise. The comparisons are made assuming the transmitter to have perfect knowledge of the channel state information (CSI) or when no CSI is available. We provide the results in terms of achievable rate (referred to capacity in the follows), which is the channel capacity [9] under the assumption of Gaussian background noise. In [8], [10], other performance analysis were made assuming the channel configuration to be Δ-style at both the transmitter and the receiver ends. While in our case we consider Δ-style and star-style structures at the transmitter and the receiver, respectively. We discuss the optimal joint design of transmit and receive processing and we evaluate the capacity through simulations. Furthermore, we evaluate the performance improvement provided by the use of MIMO schemes w.r.t. SISO.

The remainder of the paper is divided as follows. In Section II, we deal with MIMO channel characterization and we present the MIMO noise model that we have derived from the experimental basis. In Section III, we present the system architecture. Then, in Section IV, we provide numerical results. Finally, the conclusions follow.

II. MIMO PLC

We study the MIMO PLC system from an experimental basis. Firstly, we describe the idea behind MIMO PLC. Then, we propose a concise statistical characterization of the MIMO channel frequency response. Finally, we present a model for the covariance of the MIMO noise. In this respect, we remark that while the channel analysis is based on the knowledge of the actual measured channel responses, the noise model has been derived from the main findings reported by the STF-410 and in [8].

A. Principle

When more than two conductors are present, multiple communications can be established. In general, due to Kirchhoff's laws, with N conductors, only $N-1$ channels are available for transmission. Otherwise, all the 4 star-style receiving modes can be used, providing a noticeable channel gain. We follow the approach that was proposed by STF-410, showing the MIMO modes that we consider in Fig. 1. Basically, we signal differentially between pairs of wires P, N and E, namely, PN, PE and NE, and we receive between P or N or E and the reference plane. To enforce the physical earth path, at the receiver, the coupler is connected to a ground plate of approximately one squared-meter area. In this respect, we note that flat TVs are equipped with big metal backplanes that can act as the ground plate [11]. Thus, the CM can be used as a further received signal in order to obtain a 2×4 MIMO communication system. The feeding and receiving configurations are referred to as Δ and star, respectively. We denote the Δ-style modes PN, PE, NE with Δ_1, Δ_2, Δ_3, the star-style modes P, N, E with s_1, s_2, s_3, and CM with s_4. We focus on the feeding modes Δ_1 and Δ_2 and on all star-style plus CM receiving modes.

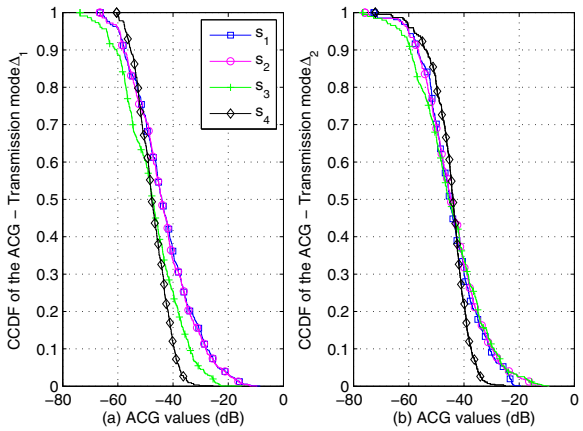

Fig. 2. CCDF of the average channel gain as a function of the MIMO modes. From left to right, results for Δ_1 and Δ_2 transmission modes are shown.

B. Channel Frequency Response

We contributed to the experimental measurement campaign that was performed by STF-410 across Europe to collect information about MIMO channels. A total amount of 353 MIMO channels were acquired. For further details the reader is referred to [2].

Measurements were performed in the frequency domain, according to the measurement procedure that is detailed in [2] and that was followed by all members of STF-410 to collect data. We collected 1601 samples of the scattering parameters in the 1–100 MHz frequency range, for each one of the 353 acquired MIMO channels. Therefore, the resolution in frequency is $\Delta f = 61.875$ kHz. In this work, we focus on the 2–86 MHz frequency range, as specified by the HomePlug AV2 standard [1], and we define the channel frequency response (CFR) as the scattering parameter s_{21}. $H_{s_r,\Delta_t}(f)$ denotes the CFR between the Δ-style port t and the star-style port r at frequency f, where $t = 1, 2$ and $r = 1, 2, 3, 4$. Hence, the 4×2 CFR matrix $\mathbf{H}(f)$ is defined, and the tr-th element of $\mathbf{H}(f)$ is $H_{s_r,\Delta_t}(f)$.

We investigate the statistics of the measured channels. Firstly, we focus on the average channel gain (ACG) that is computed as follows

$$G_{s_r,\Delta_t} = 10\log_{10}\left(\frac{1}{N}\sum_{i=N_1}^{N_2}|H_{s_r,\Delta_t}(i\Delta f)|^2\right) \quad [dB], \quad (1)$$

where $N_1\Delta f = 2$ MHz, $N_2\Delta f = 86$ MHz and $N = N_2 - N_1$. Fig. 2 shows the complementary cumulative distribution

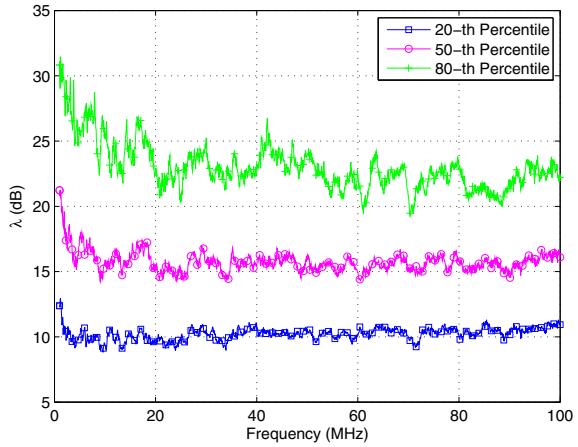

Fig. 3. 20-th, 50-th and 80-th percentile of the eigen-spread as a function of the frequency.

function (CCDF) of the ACG as a function of the signaling mode. We note the followings. First, in terms of ACG, s_1 and s_2 are equivalent. Second, when the transmission mode is Δ_1, the ACG of s_3 is 3 dB less than that of s_1 and s_2. Indeed, when the transmission mode is Δ_2, the distribution of the ACG of s_3 is close to that of s_1 and s_2. Third, the ACG of s_4 is less spread than that of other receiver modes. Indeed, the ACG of the other modes spans up to -20 dB. Finally, the ACG of s_4 behaves similarly regardless the transmission mode. Note that the values in Fig. 2 concern an average gain, as in (1), and not the effective CFR gain.

Now, we perform the analysis of the singular value decomposition (SVD) of the channels in terms of eigen-spread. The SVD of the channel matrix $\mathbf{H}(f)$ reads

$$\mathbf{H}(f) = \mathbf{U}(f)\mathbf{D}(f)\mathbf{V}^H(f), \tag{2}$$

where $\mathbf{V}$ and $\mathbf{U}$ are unitary matrices, $\mathbf{D}(f)$ contains the singular values of $\mathbf{H}(f)$, and $\{\cdot\}^H$ denotes the hermitian operator. The channel matrix $\mathbf{H}$ is a 4×2 matrix, therefore, the maximum number of singular values is 2. We denote the singular values of $\mathbf{H}(f)$ with $d_i(f)$, where $i = 1, 2$, and we define the eigen-spread as $\lambda(f) = d_1(f)/d_2(f)$ [8]. Without loss of generality, we assume $d_1(f) > d_2(f)$, computing λ for all channels and frequencies to obtain its statistics. Fig. 3 depicts 20-th, 50-th and 80-th λ percentiles, in dB terms, as a function of frequency. We note that the channels are slightly more correlated in the lower frequency range, where λ is more spread. Instead, the 20-th percentile is frequency independent.

C. Noise

The analysis of Section IV requires the knowledge of the covariance matrix of the noise experienced by the star-style modes. In this respect, we propose a model that exploits the experimental evidence reported in [7] and [8]. We proceed as follows. We assume the noise to be Gaussian with zero mean, we focus on the frequency domain, and we denote the covariance between the noise of the modes s_i and s_j with $R_{ij}(f) = E[N_{s_i}(f)N^*_{s_j}(f)]$, where $i, j = 1, \ldots, 4$ and $N_{s_i}(f)$ is the Fourier transform of the noise experienced by the mode s_i. We let the main-diagonal elements of the covariance matrix, namely, $R_{ii}(f)$, be equal to the power spectral density (PSD) of the measured noise. In this respect, we exploit the results provided by STF-410 in [7]. CM experiences the highest noise. According to [7], the auto-correlation of mode CM, i.e. $R_{44}(f)$, is approximately 5 dB greater than the noise of the other modes.

Now, we focus on the cross-correlation terms, i.e., $R_{ij}(f)$ with $i \neq j$. The noise received on different ports is correlated [7]. Therefore, $R_{ij}(f) \neq 0$. We model the covariance matrix element $R_{ij}(f)$ as

$$R_{ij}(f) = \alpha_{ij} \left(R_{ii}(f) + R_{jj}(f) \right), \tag{3}$$

where α_{ij} is a constant coefficient that can be obtained as follows. We validate the model proposed in (3) starting from the correlation coefficient [8]

$$\Phi_{ij}(f) = \frac{\left| R^{\Delta}_{ij}(f) \right|}{\sqrt{R^{\Delta}_{ii}(f) R^{\Delta}_{jj}(f)}}, \tag{4}$$

where $R^{\Delta}_{ij}(f) = E[N_{\Delta_i}(f) N^*_{\Delta_j}(f)]$ is the covariance between the noise of the modes Δ_i and Δ_j, with $i, j = 1, 2$. Note that $N_{\Delta_1}(f) = N_{s_1}(f) - N_{s_2}(f)$, and similar relations hold for the other Δ mode noise terms. In [8], it is shown that $\Phi_{ij}(f)$, as well as $R^{\Delta}_{ii}(f)$, exhibit approximately the same frequency-decreasing profile regardless the pair of considered modes. Therefore, we speculate that $R^{\Delta}_{12}(f)$, $R^{\Delta}_{13}(f)$ and $R^{\Delta}_{23}(f)$ differ by a constant value from each other. Now, let us compute

$$R^{\Delta}_{12}(f) - R^{\Delta}_{13}(f) = R_{11}(f) + R_{22}(f) - 2\mathrm{Re}\{R_{12}(f)\}, \tag{5}$$

where $\mathrm{Re}\{\cdot\}$ denotes the real operator. We note that the left side of (5) is a constant value, regardless frequency. Therefore, both sides of relation (5) are frequency independent, and $R_{12}(f)$ should compensate the frequency variations due to $R_{11}(f)$ and $R_{22}(f)$. We extend the conclusion to all star-style modes. This proves the model in (3).

Now, we focus on the coefficient α_{ij}. We introduce the time domain correlation coefficient ϕ_{ij}, i.e., [7]

$$\begin{aligned} \phi_{ij} &= \frac{E[n_{s_i}(t) n_{s_j}(t)] - m_{s_i} m_{s_j}}{\sqrt{\sigma^2_{s_i} \sigma^2_{s_j}}} \\ &= \frac{\int R_{ij}(f) df}{\sqrt{\int R_{ii}(f) df \int R_{jj}(f) df}}, \end{aligned} \tag{6}$$

where m_{s_i} and $\sigma^2_{s_i}$ are the mean and the variance of the noise $n_{s_i}(t)$ (in the time domain) experienced by mode s_i. Hence, we substitute (3) in (6) and we obtain

$$\alpha_{ij} = \phi_{ij} \frac{\sqrt{\int R_{ii}(f) df \int R_{jj}(f) df}}{\int R_{ii}(f) df + \int R_{jj}(f) df}, \tag{7}$$

where ϕ_{ij} is the time domain correlation coefficient that we define as in [7]. We generate ϕ_{ij} randomly, according to the statistics that was presented in [7].

III. System Model

We consider an OFDM-MIMO PLC channel with n_T transmit and n_R receive signals. For each sub-carrier i, the general processing scheme is shown in Fig. 4.

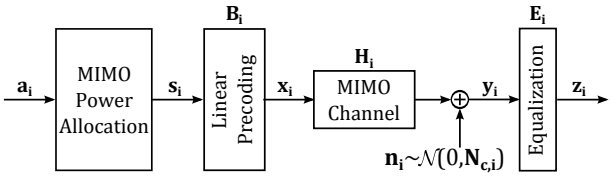

Fig. 4. MIMO PLC coding scheme of the i-th sub-carrier.

The n_T transmitted symbols of the i-th frequency (expressed by the $n_T \times 1$ vector $\mathbf{a_i}$) are weighted by the power allocation coefficients and precoded by the $n_T \times n_T$ matrix $\mathbf{B_i}$ (beamforming), yielding the $n_T \times 1$ transmitted signal $\mathbf{x_i}$.

We assume uncorrelated with zero mean and unit energy symbols (i.e., $E[\mathbf{a_i}{\mathbf{a_i}}^H] = \mathbf{I}_{n_T}$, the $n_T \times n_T$ identity matrix). Thus, the matrix $\mathbf{Q_i} = E[\mathbf{s_i}{\mathbf{s_i}}^H]$ of the signal $\mathbf{s_i} = {\mathbf{Q_i}}^{1/2}\mathbf{a_i}$ is diagonal and represents the power allocation of the total available power P_T. In our system $P_T = P_i$, where P_i is the power spectral density mask at the i-th carrier.

At each frequency, the $n_R \times 1$ received signal $\mathbf{y_i}$ on the i-th sub-carrier is equal to

$$\mathbf{y_i} = \mathbf{H_i}\mathbf{x_i} + \mathbf{n_i}, \tag{8}$$

where $\mathbf{n_i} \sim \mathcal{N}(0, \mathbf{N_{c,i}})$ is the $n_R \times 1$ additive Gaussian noise with zero mean and covariance matrix $\mathbf{N_{c,i}} = E[\mathbf{n_i}{\mathbf{n_i}}^H]$. The noise is colored in frequency and correlated in the spatial domain (see Section II-C). At the receiver, $\mathbf{y_i}$ is equalized by the $n_T \times n_R$ matrix $\mathbf{E_i}$ to yield the $n_T \times 1$ detected vector $\mathbf{z_i}$. For the OFDM transmission system the capacity can be computed as [9]

$$C = \sum_{i \in \mathcal{I}_{ON}} \log_2 \left[\det \left(\mathbf{I}_{n_R} + {\mathbf{N_{c,i}}}^{-1} \mathbf{H_i} \mathbf{\Phi_i} {\mathbf{H_i}}^H \right) \right], \tag{9}$$

where $\mathcal{I}_{ON}$ is the set of all active sub-carriers and $\mathbf{\Phi_i} = E[\mathbf{x_i}{\mathbf{x_i}}^H]$ is the covariance matrix of the transmitted signal. We assume a sufficiently high number of sub-channels so that the cyclic prefix (CP) effect can be neglected.

A. Full Knowledge of the CSI at the Transmitter

The optimal processing scheme assumes perfect knowledge of the channel response and the noise covariance matrix at the transmitter side [12]. When this information is available, we can allocate the total transmit power in the most efficient way as follows. First, we whiten the noise by pre-multiplying the received signal by ${\mathbf{N_{c,i}}}^{-1/2}$, where ${\mathbf{N_{c,i}}}^{-1} = {\mathbf{N_{c,i}}}^{-1/2} \left({\mathbf{N_{c,i}}}^{-1/2} \right)^*$. We obtain

$${\mathbf{N_{c,i}}}^{-1/2}\mathbf{y_i} = \mathbf{H_{o,i}}\mathbf{x_i} + \mathbf{w_i}, \tag{10}$$

where $\mathbf{H_{o,i}} = {\mathbf{N_{c,i}}}^{-1/2}\mathbf{H_i}$ is the resulting channel matrix (which combines the effect of noise correlation and the channel attenuation), and $\mathbf{w_i} \sim \mathcal{N}(0, \mathbf{I}_{n_R})$ is the AWGN noise.

Then, we compute the SVD of the matrix $\mathbf{H_{o,i}}$, i.e. $\mathbf{H_{o,i}} = \mathbf{U_{o,i}}\mathbf{D_{o,i}}{\mathbf{V_{o,i}}}^H$ and we exploit the water-filling algorithm to obtain the optimal power allocation. The optimal precoding matrix $\mathbf{B_i}$ is the unitary matrix $\mathbf{V_{o,i}}$ [12]. Hence, the optimal transmitted signal covariance matrix reads $\mathbf{\Phi_{o,i}} = \mathbf{V_{o,i}}\mathbf{Q_{o,i}}{\mathbf{V_{o,i}}}^H$. At the receiver, after the whitening filter, we apply zero-forcing equalization with matrix

$${\mathbf{H_{o,i}}}^\dagger = \left({\mathbf{H_{o,i}}}^H \mathbf{H_{o,i}} \right)^{-1} {\mathbf{H_{o,i}}}^H, \tag{11}$$

where ${\mathbf{H_{o,i}}}^\dagger$ is the pseudo inverse of the channel matrix $\mathbf{H_{o,i}}$. With the optimal allocation strategy and linear precoding scheme, the MIMO PLC channel capacity in (9) becomes

$$C = \sum_{i \in \mathcal{I}_{ON}} \log_2 \left[\det \left(\mathbf{I}_{n_R} + \mathbf{D_{o,i}}\mathbf{Q_{o,i}}{\mathbf{D_{o,i}}}^H \right) \right], \tag{12}$$

where the MIMO channel has been diagonalized into $r = \text{rank}(\mathbf{H_i})$ parallel spatial sub-channels because $\mathbf{D_{o,i}}$ is a diagonal matrix. In our channels, the multiplexing order is $r = \min(n_T, n_R) = 2$.

B. No Knowledge of the CSI at the Transmitter

When the transmitter has no knowledge about the channel, the optimal power distribution is the uniform one ($\mathbf{\Phi_i} = P_T/n_T \mathbf{I}_{n_T}$). In this case, no linear precoding is possible ($\mathbf{B_i} = \mathbf{I}_{n_T}$). Furthermore, at the receiver side, zero-forcing detection is accomplished according to (11) where we substitute $\mathbf{H_{o,i}}$ with $\mathbf{H}_i$. The capacity turns into

$$C = \sum_{i \in \mathcal{I}_{ON}} \log_2 \left[\det \left(\mathbf{I}_{nR} + \frac{P_i}{n_T} {\mathbf{N_{c,i}}}^{-1} \mathbf{H_i} {\mathbf{H_i}}^H \right) \right], \tag{13}$$

where P_i is the power (in Watt) drawn from the PSD constraint on the i-th sub-carrier.

IV. Numerical Results

In this Section, we discuss the performance of the coding schemes when the transmitter has perfect knowledge about the CSI and when it does not have any CSI information. Further, we compare the performances of different MIMO configurations. We provide the results in terms of capacity, that we compute as described in Section III. To this aim, we fulfill the specifications of the HomePlug AV2 standard [1]. Namely, we consider the frequency range 2–86 MHz with a PSD limit of -50 dBm/Hz and -80 dBm/Hz in the range 2–30 MHz and 30–86 MHz, respectively. This is a constraint on the total transmit power per carrier, which could be divided among the different Δ-style transmissions modes. Furthermore, the noise is assumed to be colored in frequency and spatially correlated, among the different star-style receiving modes, according to the model described in Section II-C.

Fig. 5 shows the differences between the capacity distribution achieved when the transmitter has perfect CSI knowledge (channel matrix $\mathbf{H_i}$ and noise covariance matrix $\mathbf{N_{c,i}}$ for all $i \in \mathcal{I}_{ON}$) and when no CSI is available at the transmitter side. For both cases the optimal power allocation scheme has been implemented (water-filling and uniform, respectively). The two curves appear to almost overlap, but this is not true for low target rates, indeed the average difference in capacity, among all the considered realizations, is in the order of tens of megabits (10 Mb/s). Instead, the two curves actually overlap each other for high target rates (achieved with low probabilities). This is due to the high signal-to-noise ratio (SNR) in the range 2–30 MHz which involves the optimal power allocation to be uniform. Thus, the capacity increase,

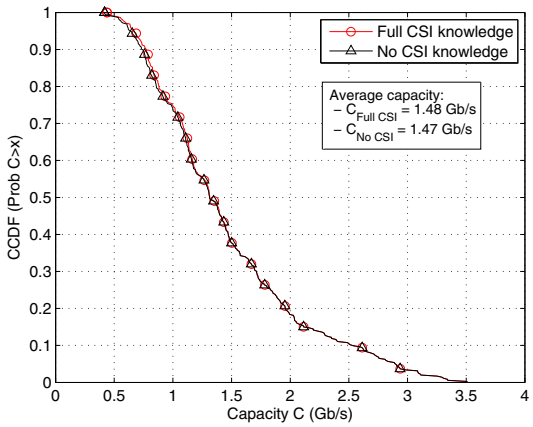

Fig. 5. Capacity CCDF with and without the CSI knowledge at the transmitter assuming 2×4 case. The average achieved capacity is also reported.

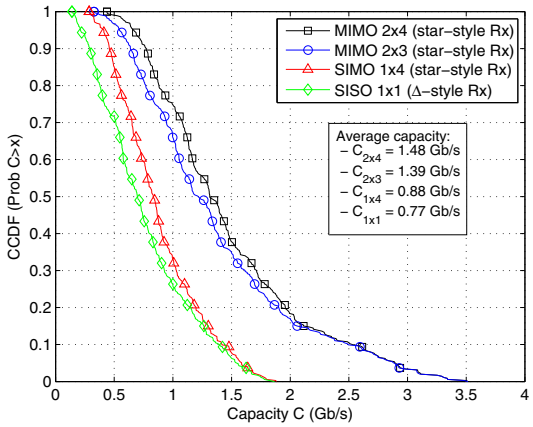

Fig. 6. Capacity distribution comparison among SISO, SIMO and MIMO system configurations when all or some of the available ports are used.

due to CSI knowledge at the transmitter, becomes significant in the range 30–86 MHz (affected by low SNR) and is roughly 0.63% in our simulations. The results in Fig. 5 suggest that for high SNRs the feedback of the CSI and its overhead, as well as the linear precoding (beamforming) at the transmitter, could be avoided through the use of uniform power allocation, yet yielding high rates. This translates into a complexity reduction.

The advantages provided by MIMO w.r.t. SIMO and SISO are depicted in Fig. 6. Concerning MIMO, we feed two Δ-style modes and we receive all, or some, of the star-style modes. Instead, in the SIMO configuration we feed only Δ_1, whereas in the SISO implementation we assume that both the transmitter and the receiver are configured in Δ mode. As Fig. 6 shows, the larger the number of used ports by both sides (Tx and Rx), the greater the capacity. In particular, it can be noted a significant increase in capacity going from single-input to multiple-input systems, taking into account multiple-output configuration. This is due to the doubling of the multiplexing order (or rank of the channel matrix) from 1 to 2. Furthermore, the 2×4 MIMO case (HomePlug AV2 standard) approximately doubles the capacity of the SISO scheme (HomePlug AV). This is a significant improvement, compared to conventional SISO systems, in order to meet the increasing demand of high speed multimedia data exchange.

V. Conclusions

We have discussed the use of MIMO schemes in PLC when additive colored and correlated Gaussian noise is present. We have compared the capacity performance between different coding schemes that exploit CSI to perform the optimal spatial allocation of the available power. The simulation results shows that the CSI knowledge translates into a significant increase in performances only for bad channel realizations and low SNR. For high SNR, the uniform allocation is optimal and no CSI feedback is required. Further, we have shown that the increase in capacity, due to the exploitation of all the possible transmit and receive ports (2×4 in our case), outperforms any other coding scheme. Particularly, the 2×4 MIMO experimental channels analyzed achieve a capacity that almost doubles that of a conventional SISO scheme.

References

[1] L. Yonge, J. Abad, K. Afkhamie, L. Guerrieri, S. Katar, H. Lioe, P. Pagani, R. Riva, D. Schneider, and A. Schwager, "An Overview of the HomePlug AV2 Technology," to appear in *Journal of Electrical and Computer Engineering*, 2013.

[2] ETSI TR 101 562-1 V 1.3.1, "PowerLine Telecommunications (PLT); MIMO PLT; Part 1: Measurement Methods of MIMO PLT," European Telecommunication Standardization Institute, Tech. Rep., 2012.

[3] L. Stadelmeier, D. Schill, A. Schwager, D. Schneider, and J. Speidel, "MIMO for Inhome Power Line Communications," in *Proc. of 7th International ITG Conference on Source and Channel Coding (SCC 2008)*, 2008, pp. 1–6.

[4] D. Schneider, J. Speidel, L. Stadelmeier, and D. Schill, "Precoded Spatial Multiplexing MIMO for Inhome Power Line Communications," in *Proc. of IEEE Global Telecommunications Conference (GLOBECOM 2008)*, 2008, pp. 1–5.

[5] D. Schneider, A. Schwager, J. Speidel, and A. Dilly, "Implementation and Results of a MIMO PLC Feasibility Study," in *Proc. of IEEE Int. Symp. on Power Line Commun. and Its App. (ISPLC 2011)*, 2011, pp. 54–59.

[6] R. Hashmat, P. Pagani, A. Zeddam, and T. Chonavel, "MIMO Communications for Inhome PLC Networks: Measurements and Results up to 100 MHz," in *Proc. of IEEE Int. Symp. on Power Line Commun. and Its App. (ISPLC 2010)*, 2010, pp. 120–124.

[7] ETSI TR 101 562-3 V 1.1.1, "PowerLine Telecommunications (PLT); MIMO PLT; Part 3: Setup and Statistical Results of MIMO PLT Channel and Noise Measurements," European Telecommunication Standardization Institute, Tech. Rep., 2012.

[8] D. Rende, A. Nayagam, K. Afkhamie, L. Yonge, R. Riva, D. Veronesi, F. Osnato, and P. Bisaglia, "Noise Correlation and Its Effect on Capacity of In-home MIMO Power Line Channels," in *Proc. of IEEE Int. Symp. on Power Line Commun. and Its App. (ISPLC 2011)*, April 2011, pp. 60–65.

[9] B. Holter, "On the Capacity of the MIMO Channel: A Tutorial Introduction," in *Proc. of IEEE Norwegian Symp. on Signal Processing*, Trondheim, Norway, 18-20 October 2001, pp. 167–172.

[10] A. Canova, N. Benvenuto, and P. Bisaglia, "Receivers for MIMO-PLC Channels: Throughput Comparison," in *Proc. of IEEE Int. Symp. on Power Line Commun. and Its App. (ISPLC 2010)*, March 2010, pp. 114–119.

[11] A. Schwager, D. Schneider, W. Baschlin, A. Dilly, and J. Speidel, "MIMO PLC: Theory, Measurements and System Setup," in *Proc. of IEEE Int. Symp. on Power Line Commun. and Its App. (ISPLC 2011)*, April 2011, pp. 48–53.

[12] D. P. Palomar, J. M. Cioffi, and M. A. Lagunas, "Joint Tx-Rx Beamforming Design for Multicarrier MIMO Channels: A Unified Framework for Convex Optimization," *IEEE Transactions on Signal Processing*, vol. 51, no. 9, pp. 2381–2401, September 2003.